THE EXTRACTION OF THE SURFACE RECOMBINATION VELOCITY OF Si:P EMITTERS USING ADVANCED SILICON MODELS

P.P. Altermatt,[1] J.O. Schumacher,[2] A.Cuevas,[3] S.W. Glunz,[2] R.R. King,[4] G. Heiser,[1,5] A. Schenk[6]

[1] Centre for Photovoltaic Engineering, University of New South Wales, Sydney, 2053, Australia, pietro@cse.unsw.edu.au
[2] Fraunhofer Institute for Solar Energy Systems, Oltmannstr. 5, 79100 Freiburg,
Germany, schum@ise.fhg.de, glunz@ise.fhg.de
[3] Centre for Sustainable Energy Systems, FEIT, Dep. of Engineering, Australian National University,
Canberra ACT 0200, Australia, Andres.Cuevas@faceng.anu.edu.au
[4] Spectrolab Inc.,12500 Gladstone Ave., Sylmar, CA 91342, USA, rking@spectrolab.com
[5] School for Computer Science and Engineering, University of NSW, Sydney, 2053, Australia, G.Heiser@unsw.edu.au
[6] Integrated Systems Laboratory, ETH Zurich, Gloriastr. 35, 8092 Zurich, Switzerland, schenk@iis.ee.ethz.ch

The recombination velocity of minority carriers at the surface of phosphorus doped emitters is re-extracted from published measurements of the emitter saturation current by means of numerical simulations. In contrast to previous studies, Fermi-Dirac statistics and a quantum mechanically derived band gap narrowing model are used (instead of Boltzmann statistics and empirical apparent BGN data). In this way, degeneracy effects are accounted for on a physical sounder basis, leading to consistency also at high dopant densities. This enables us to simulate emitters with dopant densities higher than 3×10^{19} cm^{-3} considerably more precisely than in the past.
Keywords: Modelling - 1: c-Si - 2: Passivation - 3

1. PURPOSE OF THIS WORK

The recombination at the front surface is a dominant loss in many types of solar cells. However, its quantification has been challenging. This is so because the recombination velocity of minority carriers at the emitter surface S cannot be measured directly, but the total losses in the emitter, expressed as the emitter saturation current-density J_{oe}. In order to extract S from J_{oe} measurements, the contributions to J_{oe} from the bulk of the emitter and from the surface need to be separated, using theoretical models.

In the past, various models have been used to extract S from J_{oe}. As they divide up the losses in the bulk and at the surface in different proportions, the resulting S is model-dependent. In this paper, we re-evaluate the J_{oe} measurements made by Cuevas et al. [1-3], Glunz et al. [4], and King et al. [5], using the BGN model recently developed by Schenk [6], and the silicon parameter-set established at the University of New South Wales (UNSW).

2. THE MODEL

In the extraction of S of emitters, many relevant silicon parameters and device models come into play. These are the intrinsic carrier density of silicon n_i, the statistics for the energy distribution of free carriers, band gap narrowing (BGN), Auger recombination, minority carrier mobility, the density of states (DOS) affected by doping, and incomplete ionisation of dopants. Apart from n_i, all these items are effects caused by carrier-carrier and carrier-dopant interactions. The improvements in the understanding of the emitter over past years can be regarded as a shift from the ideal-gas to many-body theory.

2.1 Fermi-Dirac instead of Boltzmann statistics
Most published calculations of solar cells are based on Boltzmann statistics, representing the ideal electron gas, because Fermi-Dirac (FD) statistics is cumbersome to include in analytical models. However, many solar cells contain performance limiting regions that are doped more highly than 1×10^{19} cm^{-3}, where degeneracy effects become significant. We therefore use FD statistics, which can be applied in numerical modelling without difficulties.

2.2 The new intrinsic carrier density of silicon
In 1991, Green and Sproul [7] lowered the most precisely measured value of n_i from 1.45×10^{10} to 1.00×10^{10} cm^{-3} (at T=300 K). Recently, it has been shown [8] that the measurements of Sproul and Green were influenced by BGN, even though the dopant density of their samples was low. This implies that $n_i = 9.65 \times 10^9$ cm^{-3}, which resolves a discrepancy with the measurement of Misiakos and Tsamakis [9]. Hence, we use the slightly lower value of $n_i = 9.65 \times 10^9$ cm^{-3} in this study.

King et al. [5] used the old $n_i = 1.45 \times 10^{10}$ cm^{-3} for calculating S. Ref. 1 contains a re-evaluation of their results applying the revised $n_i = 1.00 \times 10^{10}$ cm^{-3}. The changes in S, caused by using the slightly lower $n_i = 9.65 \times 10^9$ instead of 1.00×10^{10} cm^{-3}, are minor.

2.2 Apparent and quantum mechanically derived BGN
So far, solar cells have been mostly simulated with empirical BGN models that were derived from electronic measurements of highly doped silicon. As such BGN values were extracted from transport measurements, they are influenced by the transport model applied in the data evaluation. They do not reflect the actual band gap shrinkage ΔE_g, but are a conglomeration of various effects, such as degeneracy and changes in the DOS. Hence, such values are called 'apparent band gap narrowing' ΔE_g^{app}.

Since degeneracy effects are partly compensated for in ΔE_g^{app}, we cannot apply Fermi-Dirac statistics together with ΔE_g^{app} values, as this would overestimate degeneracy effects. Since the ΔE_g^{app} values shown in Figure 1 were obtained with various transport models, it is not obvious
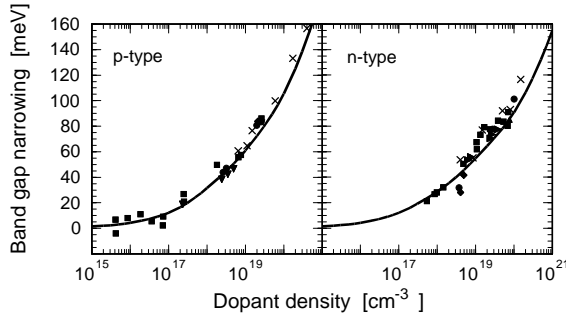
Fig. 1: Measured [15] (symbols) and calculated [6] (line) band gap narrowing as a function of phosphorus dopant density.


Fig. 2: Minority hole mobility as a function of phosphorus dopant density. The model of Klaassen [15] is modified to fit the smallest and largest measured values.

how exactly degeneracy influences ΔE_g^{app}, and we cannot correct the ΔE_g^{app} values for FD statistics with one single and well recognised procedure.

Instead, we implemented the comprehensive BGN model of Ref. 6 in the device simulator Dessis [10]. This BGN model was recently derived from quantum mechanical principles, where both carrier-carrier and carrier-dopant interactions were treated on an equal basis. Therefore, this model provides the band edge energies, E_c and E_v, separately and can be used together with FD statistics. This is a fundamentally different approach from the determination of ΔE_g^{app}. Hence, it is generally insufficient to compare solely ΔE_g of Ref. 6 with the ΔE_g^{app} values. However, at low dopant densities and under low-level injection conditions, the BGN model of Ref. 6 can be directly compared with ΔE_g^{app}, and Figure 1 shows that there is good agreement between the two approaches. In the high doping range, the model of Ref. 6 provides a similar ΔE_g as photoluminescence measurements (crosses in Fig. 1). They give a slightly higher ΔE_g than Ref. 6 due to band tails, which host immobile carriers and therefore do not contribute to BGN relevant to electronic devices. In Section 4.1 we will show that the usage of FD statistics and the BGN model of Ref. 6 give consistent results.

2.3 Auger recombination

The band-to-band Auger recombination is an intrinsic property of silicon and is usually limiting the minority excess carrier lifetime in emitters. At dopant densities N_{dop} above 1×10^{18} cm^{-3}, the Auger recombination lifetime τ_A can be described assuming non-interacting free particles, i.e. by $\tau_A = 1/C_n N_{dop}$, where C_n is the Auger coefficient. At $N_{dop} > 1 \times 10^{18}$ cm^{-3}, we use $C_n = 2.8 \times 10^{-31}$ cm^{6}s^{-1} as given by Dziewior and Schmid [11], because their data shows the smallest scatter of all the lifetime data that were published to determine C_n. In their extraction of S, Cuevas et al. took a slightly different C_n value [1-3], while King et al. also used Dziewior and Schmid's value in the emitter [12].

At $N_{dop} < 1 \times 10^{18}$ cm^{-3}, the Auger recombination rate is enhanced by Coulomb interactions [13,14], and the model of Ref. 14 is applied in this study.

2.4 Minority carrier mobility

At dopant densities found in emitters, the mobility of minority holes $\mu_{h,min}$ is limited by hole-dopant interactions in a complex way. The measured values of $\mu_{h,min}$ are shown
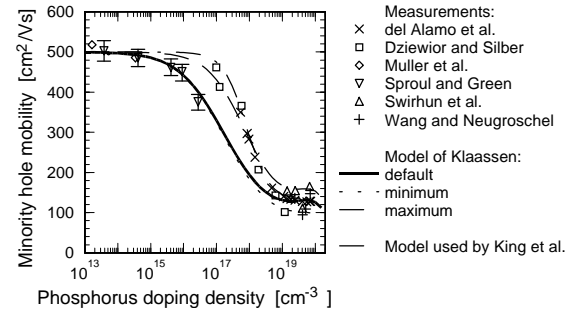
in Figure 2. They scatter by such an extent that $\mu_{h,min}$ is inducing the largest error bounds on S in our study. We adapt the model of Klaassen [15] to the experimentally determined values, as is shown in Figure 2. Cuevas et al. used a very similar model, while King's model resulted in a slightly higher mobility at $N_{dop} \approx 5 \times 10^{17}$ cm^{-3} [12].

2.5 DOS and incomplete ionisation

The influence of the impurity band and incomplete ionisation on the extracted S values is minor compared to the error bounds imposed by the scatter of the mobility data. We will report on effects caused by the DOS and incomplete ionisation elsewhere [16], as this would exceed the scope of this paper.

3. SIMULATION OF J_{oe}

We use the device simulator Dessis [10] which – in contrast to the analytical models of previous studies – solves the fully-coupled set of semiconductor differential equations numerically and in a self-consistent way. Using the models and parameters of Chapter 2, we simulate the J_{oe} measurements of Refs. 1-5 and extract S.

In analogy to the law of mass action for ideal gases, the relation $n_i^2 = np$ holds only if the carriers do not interact strongly with each other, i.e. in weakly doped silicon. Instead, Dessis calculates the electron density n using

$$n = N_c F_{1/2} \left[\frac{E_{fn} - E_c^{(0)} + \Delta E_c}{kT} \right], \quad (1a)$$

where $F_{1/2}$ is the Fermi integral of order ½, describing FD statistics. N_c is the effective density of states in the conductions band, $E_c^{(0)}$ is the energy of the intrinsic conduction band edge, which is shifted by ΔE_c due to BGN, and E_{fn} is the quasi-Fermi level for electrons. The hole density p is expressed in an analogous way as in Equation 1a. However, since the holes are non-degenerate in n-type emitters, p becomes:

$$p = N_v \exp \left[\frac{E_v^{(0)} - E_{fp} + \Delta E_v}{kT} \right] \quad (1b)$$

In order to clarify the influence of FD statistics on the simulated J_{oe}, we write the pn product in a way that n_i^2, degeneracy, band gap narrowing, and deviations from thermal equilibrium are separated by factors:

$$pn = n_i^2 \times F_{1/2}\left[\frac{E_{fn} - E_c^{(0)}}{kT}\right] \bigg/ \exp\left[-\frac{E_c^{(0)} - E_{fn}}{kT}\right]$$

$$\times F_{1/2}\left[\frac{E_{fn} - E_c^{(0)} + \Delta E_c}{kT}\right] \bigg/ F_{1/2}\left[\frac{E_{fn} - E_c^{(0)}}{kT}\right] \exp[\Delta E_v]$$

$$\times \exp\left[\frac{E_{fn} - E_{fp}}{kT}\right]$$

$$\equiv n_i^2 \times \gamma_{\deg} \times \gamma_{BGN} \times non-equilibrium \ . \qquad (2)$$

The degeneracy factor γ_{deg} is a measure of how much the electron density deviates from its classical value. If the electrons are non-degenerated as well, as is the case in lowly doped n-type emitters, we have $\gamma_{deg} \to 1$, $\gamma_{BGN} \to \exp[(\Delta E_c + \Delta E_v)/kT]$, and $pn \to n_{i,eff}^2 = n_i^2 \exp[\Delta E_g/kT]$. Equation 2 shows that, while BGN increases the *pn*-product towards the surface of the diffused emitter, degeneracy tends to decrease the *pn*-product, leading to a maximum value within the bulk. Such counteracting effects between BGN and carrier degeneracy cannot be quantified using apparent BGN data and Boltzmann statistics. For further discussions on this see Ref. 17.

In order to determine J_{oe}, we simulate the illuminated diodes of Refs. 1-5 in steady-state open-circuit conditions (the diodes have no metal contacts). We use the original SIMS data as dopant profile, and we express J_{oe} by the general definition [17]:

$$J_{oe} \equiv \frac{J_n(x_e)}{n(x_e)\,p(x_e) - n_{i,eff}^2(x_e)}\, n_{i,eff}^2(x_e) , \qquad (3)$$

This shows that J_{oe} is related at open-circuit conditions to the electron recombination current $J_n(x_e)$ at the edge x_e of the space charge region.

4. RESULTS

4.1 The measurements of Cuevas et al.

Cuevas et al. measured J_{oe} of planar emitters after applying various surface passivation treatments, and also after covering the surfaces with metal. The latter serves here as a
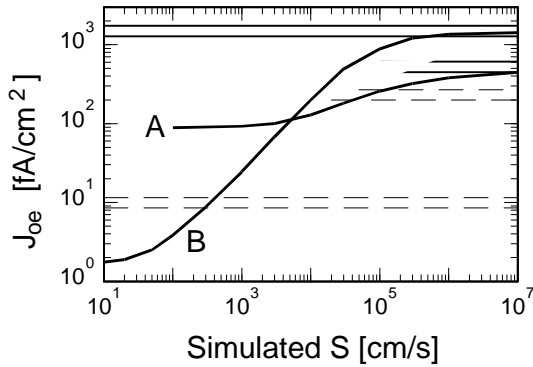
Fig. 3: Simulated J_{oe} of the highest (A) and lowliest (B) doped emitter of Cuevas et al. The error bounds of the measured J_{oe} of metal coated and oxide passivated surfaces are given by the solid and dashed lines, respectively.
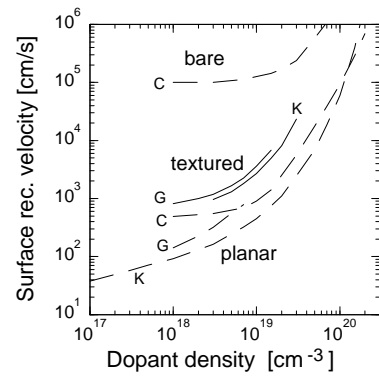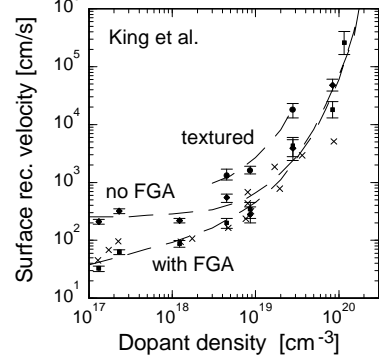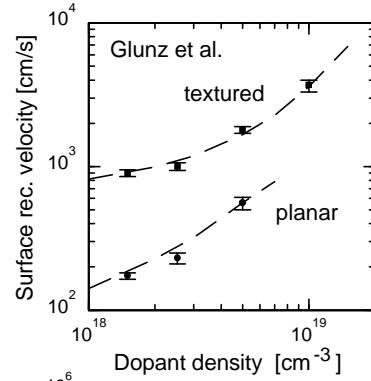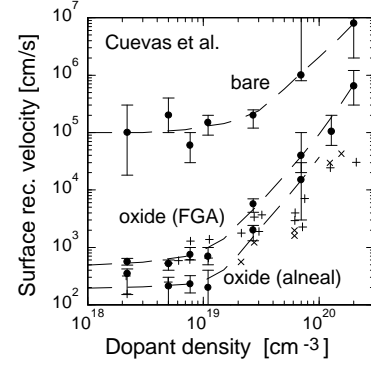
Fig. 4: Re-evaluated S (symbols with error bars), a guide to the eyes (lines), and S values from previous models (crosses).

consistency check of the model outlined in Chapter 2, because S of metal covered surfaces is limited by the thermal velocity of free carriers, i.e. $S \approx 1 \times 10^7$ cm/s. Figure 3 shows the simulated J_{oe} of both the lowliest and highest doped emitter in the study of Cuevas et al. ($N_{dop} = 2.2 \times 10^{18}$ and 2×10^{20} cm^{-3}). We can reproduce the measured J_{oe}

values of all metal covered emitters, indicating that our simulation model is consistent.

Figure 4 (top) shows the extracted S as a function of N_{dop} of emitters with either a bare surface, or passivated by an oxide with a forming gas anneal (FGA) or aluminium anneal (alneal). The crosses are the values obtained with the analytical model of Cuevas et al. [1-3]. At $N_{dop}>3\times10^{19}$ cm^{-3}, Cuevas et al. obtained a considerably lower S. This was generally experienced in previous models, because degeneracy effects were not taken fully into account, leading to overestimated bulk recombination losses that were compensated with low S values (in highly doped emitters, old models sometimes yielded negative S values).

4.2 The measurements of Glunz et al.

Glunz et al. measured J_{oe} of emitters that were fabricated in parallel on planar and textured wafers [4], enabling us to investigate the influence of surface texturing on S. Figure 4 shows S of emitters that were unaffected by inhomogeneous dopant distributions found at textured surfaces in low and shallow diffusion profiles (such effects will be discussed somewhere else [16]). Due to texturing, an approximately fivefold enhancement of S is observed, with a weak tendency to decrease at high dopant densities.

4.3 The measurements of King et al.

In their study, King et al. extracted S of planar emitters passivated by an oxide, and with or without a FGA. In addition, some textured emitters were processed in parallel. Our re-evaluation of S is shown in Figure 4. As a comparison, we have not plotted the original values of King et al., because they were obtained using the old n_i, but we show the revised values obtained with the analytical model of Cuevas [1] as crosses. Again, our S is significantly higher at high dopant densities due to degeneracy effects. At the lowest N_{dop}, the injection conditions at the surface changed during the transient measurements, and only the J_{oe} values obtained from the lowest injection levels are used here (in contrast, more highly doped emitters remained in low-injection at all times).

4.4 Comparison of the three data-sets

Figure 4 (bottom) summarises some of the dashed lines, which are a guide to the eyes. The following features become apparent:
i) Applying a FGA, King et al. obtained the lowest S, while S of Cuevas et al. seems to saturate at $N_{dop}<1\times10^{19}$ cm^{-3} to a minimum value around 600 cm/s. The S values of Glunz et al. do not experience this saturation, although they are similarly higher than King's data. It seems that in the laboratories that fabricate(d) highest-efficiency cells (Stanford and Freiburg), passivation procedures were optimised to an extent that S keeps dropping with $N_{dop}<1\times10^{19}$ cm^{-3}. This may be the reason why highest-efficiency cells, operating at 1-sun illumination, usually have optimised emitters with $N_{dop}\approx5\times10^{18}$ cm^{-3} at the surface. If S saturated at $N_{dop}<1\times10^{19}$ cm^{-3}, it would be more beneficial to dope the emitter surfaces more highly in order to reduce the hole density (i.e. the recombination losses) at the surface.
ii) The alneal technique seems to reduce S regardless of N_{dop}. This indicates that the alneal procedure passivates a certain fraction of defects which is independent of N_{dop}, i.e. that it may passivate a certain type of defect only, leaving an other type of defect unchanged. In contrast, the FGA

seems to reduce the defect density only at $N_{dop}<1\times10^{19}$ cm^{-3}, indicating that it acts either less effectively or at different types of defects than the alneal.

iii) Although King et al. achieved a lower S than Glunz et al., texturing increases their S by the same factor (approximately five). This indicates that S may rise mainly due to defects that are related to the stress in the textured crystal, which is quite unrelated to the oxide quality.

5 MAIN ADVANTAGES OF THE NEW MODEL

In contrast to models using Boltzmann statistics and apparent BGN data, degeneracy effects are accounted for on a physical sounder basis in the new model. This leads i) to consistency even at high dopant densities, as is demonstrated in Figure 3, and ii) the S values do not compensate for neglected degeneracy effects. This enables us to simulate emitters with $N_{dop}>3\times10^{19}$ cm^{-3} considerably more accurately than in the past.

[1] A. Cuevas, G. Giroult-Matlakowski, P.A. Basore, C. Dubois, R.R. King, Proc. 1st World Conference on Photovoltaic Energy Conv., IEEE (1995), p. 1446.
[2] A. Cuevas, P.A. Basore, G. Giroult-Matlakowski, C. Dubois, J. Appl. Phys. **80** (1996) 3370.
[3] A. Cuevas, P.A. Basore, G. Giroult-Matlakowski, C. Dubois, Proceedings 13th EC Photovoltaic Solar Energy Conference, Niece (1995), p. 337.
[4] S.W. Glunz, S. Sterk, R. Steenman, W. Warta, J. Knobloch, W. Wettling, Proc. 13th EC Photovoltaic Solar Energy Conference, Niece (1995), p. 409.
[5] R.R. King, A. Sinton, R.M. Swanson, IEEE Trans. El. Dev. **37** (1990) 365.
[6] A. Schenk, J. Appl. Phys. **84** (1998) 3684.
[7] A. Sproul, M. A. Green, J. Appl. Phys. **70** (1991) 846.
[8] P.P. Altermatt, A. Schenk, G. Heiser, M.A. Green, Tech. Digest of the 11th Int. Science and Eng. Conf. (PVSEC-11), Sapporo, Japan, 1999, p. 719.
[9] K. Misiakos, D. Tsamakis, J. Appl. Phys. **74** (1993) 3293.
[10] ISE Integrated Systems Engineering AG, Zurich, Switzerland, Dessis Manual 4.0, 1997; http://www.ise.ch.
[11] J. Dziewior, W. Schmid, Appl. Phys. Lett. **31** (1977) 346.
[12] R.R. King, PhD Thesis, Standford University, 1990
[13] A. Hangleiter, R. Häcker, Phys. Rev. Lett. **65** (1990) 215.
[14] P.P. Altermatt, J. Schmid, G. Heiser, A.G. Aberle, J. Appl. Phys. **82** (1997) 4938.
[15] D.B.M. Klaassen, Solid-State El. **35** (1992) 953.
[16] To be published
[17] J. Schumacher, P.P. Altermatt, G. Heiser, A. Aberle, Tech. Digest of the 11th Int. Science and Eng. Conf. (PVSEC-11), Sapporo, Japan, 1999, p. 291